RESEARCH ARTICLE

Key Points:
- Legacy borehole logs on the U.S. Beaufort margin continental shelf directly constrain the distribution of subsea permafrost
- The borehole data largely confirm the findings of seismic studies that show permafrost signatures confined to the inner shelf
- Based on gas hydrate indicators, permafrost may once have been present beneath much of the eastern U.S. Beaufort shelf

Supporting Information:
- Supporting Information S1

Correspondence to:
C. Ruppel,
cruppel@usgs.gov

Subsea ice-bearing permafrost on the U.S. Beaufort Margin: 2. Borehole constraints

Carolyn D. Ruppel[1], Bruce M. Herman[2], Laura L. Brothers[1], and Patrick E. Hart[3]

[1]U.S. Geological Survey, Woods Hole, Massachusetts, USA, [2]Bureau of Ocean Energy Management, Anchorage, Alaska, USA, [3]U.S. Geological Survey, Santa Cruz, California, USA

Abstract Borehole logging data from legacy wells directly constrain the contemporary distribution of subsea permafrost in the sedimentary section at discrete locations on the U.S. Beaufort Margin and complement recent regional analyses of exploration seismic data to delineate the permafrost's offshore extent. Most usable borehole data were acquired on a ~500 km stretch of the margin and within 30 km of the contemporary coastline from north of Lake Teshekpuk to nearly the U.S.-Canada border. Relying primarily on deep resistivity logs that should be largely unaffected by drilling fluids and hole conditions, the analysis reveals the persistence of several hundred vertical meters of ice-bonded permafrost in nearshore wells near Prudhoe Bay and Foggy Island Bay, with less permafrost detected to the east and west. Permafrost is inferred beneath many barrier islands and in some nearshore and lagoonal (back-barrier) wells. The analysis of borehole logs confirms the offshore pattern of ice-bearing subsea permafrost distribution determined based on regional seismic analyses and reveals that ice content generally diminishes with distance from the coastline. Lacking better well distribution, it is not possible to determine the absolute seaward extent of ice-bearing permafrost, nor the distribution of permafrost beneath the present-day continental shelf at the end of the Pleistocene. However, the recovery of gas hydrate from an outer shelf well (Belcher) and previous delineation of a log signature possibly indicating gas hydrate in an inner shelf well (Hammerhead 2) imply that permafrost may once have extended across much of the shelf offshore Camden Bay.

1. Introduction

Some contemporary Arctic Ocean continental shelves host subsea permafrost that originally formed in subaerially exposed tundra (in unglaciated areas [e.g., *Romanovskii et al.*, 1998; *Hunter and Hobson*, 1974; *Hunter et al.*, 1978; *Rekant et al.*, 2005; *Brothers et al.*, 2012; *Portnov et al.*, 2013, 2014]) or beneath glaciers (e.g., Norwegian margin [*Portnov et al.*, 2016]) in Late Pleistocene time. With the end of the last glaciation and subsequent sea level rise of up to ~120 m [*Fairbanks*, 1989], these areas have now been inundated. Ocean temperatures at the seafloor are warmer than the subaerial/subglacial temperatures that persisted during formation of the permafrost [e.g., *Shakhova et al.*, 2010], and remaining subsea permafrost is believed to be rapidly thawing [*Rachold et al.*, 2007] as warmer temperatures propagate into the sedimentary section.

In recent years, studies in some parts of the Western and Eastern Arctic Oceans have constrained the offshore extent of geophysically detectable subsea permafrost to be at most only a few tens of kilometers [e.g., *Brothers et al.*, 2012; *Portnov et al.*, 2013]. In the coming decades, the Arctic amplification effect, a climate phenomenon characterized by enhanced warming at high latitudes relative to temperate zones [e.g., *Bekryaev et al.*, 2010; *Pithan and Mauritsen*, 2014], will likely contribute to continued rapid thawing of remaining subsea permafrost [e.g., *Rachold et al.*, 2007]. In newly thawed sediments, organic carbon will feed methane production, potentially leading to new methane releases from the seafloor. Subsea permafrost can also be associated with methane hydrates, and these are expected to dissociate and release gas into the surrounding sediments as thawing continues [e.g., *Paull et al.*, 2007; *Shakhova et al.*, 2010; *Ruppel*, 2011; *Portnov et al.*, 2013, 2014].

A key challenge for determining the impact of ongoing and future climate warming on subsea permafrost is the lack of information about its contemporary distribution. In the Western Arctic, ice-bearing permafrost (IBPF) on the Canadian Beaufort margin has been mapped since the 1970s using seismic refraction methods and borehole data [e.g., *Hunter and Hobson*, 1974; *Hunter et al.*, 1978; *Hu et al.*, 2013; *Kang et al.*, 2015]. The
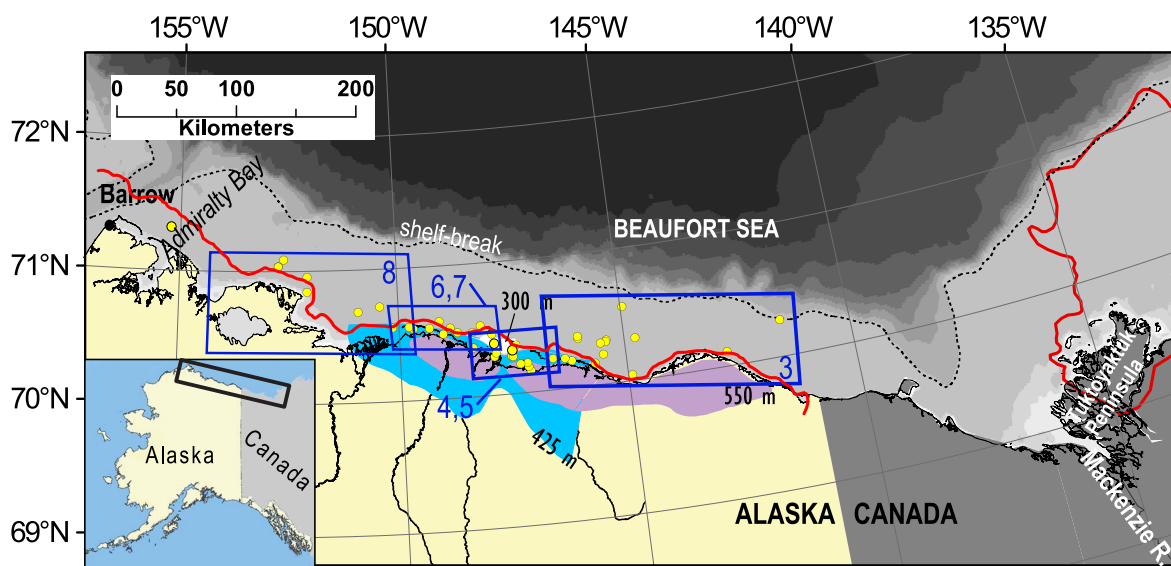
Figure 1. Map of the Beaufort Sea margin, showing the borehole well data set (yellow circles) used for this paper. The red curves on the U.S. and Canadian Beaufort margin show the inferred extent of subsea IBPF based on velocity analyses of seismic reflection data on the U.S. margin [*Brothers et al.*, 2016] and seismic refraction analyses on the Canadian margin [*Hunter et al.*, 1978], respectively. The black dashed line indicates the nominal shelf-break at 100 m water depth, which was the assumed seaward extent of subsea permafrost in the compilation of *Brown et al.* [1997]. The blue boxes indicate the locations of subsequent figures with their corresponding numbers. The blue and purple areas onshore in the central part of the Alaskan North Slope are contours showing the depth to the base of IBPF as determined by *Collett et al.* [1989]. These are labeled in units of meters, converted from the original feet. Inset: Location of this map on the Alaskan-Canadian Beaufort margin.

distribution of subsea permafrost on this part of the margin—little remaining west of the Mackenzie River and permafrost extending to nearly the shelf-break east of the Mackenzie River offshore the Tuktoyaktuk peninsula (Figure 1)—influenced a generation of researchers who subsequently assumed that subsea permafrost might currently persist to the edge of the continental shelf around much of the Arctic Ocean [*Brown et al.*, 1997].

Despite early studies hinting that subsea permafrost might be confined nearer the shore on the U.S. Beaufort margin [*National Research Council (NRC), Marine Board*, 1983] than on the Canadian margin, the first regional-scale analysis in this area was only completed in the last few years. Following *Hunter and Hobson* [1974] and *Neave and Sellman* [1984], *Brothers et al.* [2012] used seismic refraction analyses to delineate the minimum offshore extent of subsea IBPF, demonstrating that the most robust indicators for its presence were largely confined to the central U.S. Beaufort margin and nowhere extended more than 20 km offshore, nor beyond the 30 m isobath. Using analyses that determine bulk velocities in the uppermost 750 ms (two-way travel time) after data stacking, a subsequent study [*Brothers et al.*, 2016] has expanded the along-margin extent of subsea IBPF to include a thin zone that borders nearly the entire U.S. Beaufort margin (Figure 1). However, they found little evidence that the IBPF signal extends much farther seaward than the previously established isobath [*Brothers et al.*, 2012].

This paper presents the first compilation of direct borehole constraints on subsea IBPF distribution on the U.S. Beaufort Sea margin based on a comprehensive analysis of well logging data. The results in this paper complement the recent seismic-based analyses [*Brothers et al.*, 2012, 2016] and provide a data set comparable to the borehole interpretations developed for the Canadian part of this margin [e.g., *Hu et al.*, 2013]. The analysis also extends to the offshore area the mostly onshore interpretations by *Collett et al.* [1989], who contoured the base of IBPF in the central part of the Alaskan North Slope (ANS) near Prudhoe Bay (Figure 1).

2. Data and Methods

The wells used for this study (Table 1 and Supporting Information Table S1) have publicly available borehole logs acquired in federal (Outer Continental Shelf or OCS) and state wells offshore the ANS starting in the 1970s and ending in the early 2000s. The state well data and the well reports are available from the Alaska

Table 1. Wells That May Contain IBPF Signatures Based on the Resistivity Logs[a]

Well Name	Location	API Number	Latitude (N)	Longitude (W)	Deep Resistivity Log[b]	Sonic Log[c]	Figure Number	Confidence[d]
Foggy Island Bay State 1	Shoreline	50-029-20146	70.288	−147.904	x	x	2	1
Fireweed (OCS Y-0267)	Seaward of Antares wells	55-232-00003	71.088	−152.603	x		8b,S12	4
Antares 2 (OCS Y-0280-2)	Offshore west of Cape Halkett	55-232-00002	71.036	−152.724	x	x	8c,S13	3
Antares 1 (OCS Y-0280-1)	Offshore west of Cape Halkett	55-232-00001	71.036	−152.724	x	x	8d,S13	3
Orion (OCS Y-0804)	Offshore Cape Halkett	55-231-00003	70.956	−152.063	x	x	8e,S14	3
Mukluk (OCS Y-0334)	Offshore Harrison Bay	55-231-00001	70.683	−150.920	o	x	8f,S14	3
Thetis Island	Offshore Colville River Delta	50-103-20190	70.554	−150.153	x		6b,S7	1
Nikaitchuq 2	Spy Islands	50-629-23199	70.554	−149.775	o		6c,S7	1
Northwest Milne Point	Lagoon behind Spy/Jones Islands	50-029-22231	70.538	−149.682	x	x	6d,S7	1
Jones Island	Former Bodfish Island	50-029-22319	70.537	−149.319	o	x	6e,S8	1
Long Island	Jones Island chain	50-029-21043	70.487	−149.018	x	x	6f,S8	1
Sandpiper 1 (OCS Y-0370)	Seaward of strip barriers	55-201-00007	70.585	−149.097	x	x	7a,S9	2
Northstar 1	Seaward of strip barriers	50-029-21134	70.528	−148.856	x	x	7b,S9	2
Seal Island 1 (BF-47)	Seaward of strip barriers	50-029-20954	70.492	−148.693	x	x	7c,S10	1
Gull Island State 2	Prudhoe Bay	50-029-20195	70.366	−148.364	x	x	7d,S10	1
Reindeer Island	Midway Chain	50-029-20342	70.485	−148.359	x		7e,S11	1
No Name Island	Cross Island	50-029-20469	70.461	−147.935	x	x	7f,S11	1
Beechey Pt #2 (OCS Y-191-2)	Sag River outfall	55-201-00002	70.387	−147.891	x	x	4b,S3	2
Duck Island 1	Sag River outfall, barrier island	50-029-20280	70.317	−147.863	x	x	5a,S5	1
Tern A1 (OCS Y-0195)	Foggy Island Bay	55-201-00003	70.284	−147.535	o	x	4c,S3	2
Karluk	Foggy Island Bay	50-629-21897	70.325	−147.506	o	x	4e,S4	2
Liberty (OCS Y-0165)	Near Tern A1	55-201-00009	70.279	−147.496	o		4d,S4	2
West Mikkelsen 4	Shaviovik River outfall	50-029-20911	70.218	−147.347	x		5b	1
West Mikkelsen 2	On Tigvariak Island	50-029-20357	70.222	−147.190	x	x	5c,S5	1
Badami 2	East of Tigvariak Island	50-029-22230	70.192	−147.172	o	x	5d,S6	1
Badami 5	Nearshore east of Tigvariak Island	50-629-22533	70.161	−147.132	o	x	5e,S6	1
Challenge Island	Maguire Islands (east)	50-089-20012	70.236	−146.618	x	x	3b,S1	2
Alaska State F1	North Star Island, Maguire chain	50-089-20019	70.227	−146.360	x	x	3c,S1	2
Alaska State D1	Flaxman Island	50-089-20015	70.203	−146.207	x	x	3d,S1	2
Hammerhead 2 (OCS Y-0849-2)	Inner/mid-shelf offshore Flaxman	55-171-00006	70.378	−146.031	o		3f,S2	4, hydrate?
Wild Weasel (OCS Y-1597)	Offshore Camden Bay	55-171-00011	70.223	−145.499	o		3e,S2	4
Belcher (OCS Y-0197)	Outer shelf near U.S.-Canada border	55-141-00005	70.275	−141.513	LLD > 600	x	3g	Hydrate

[a]Hammerhead 2 and Belcher are included owing to the possibility of gas hydrate in these wells. Foggy Island Bay State 1 is an onshore well from *Collett et al.* [1989].
[b]The deep resistivity log is ILD if indicator is *x* and another type of resistivity/conductivity log for *o*.
[c]Sonic log is only indicated if there is coverage within the IBPF zone.
[d]Confidence gives a subjective measure indicating (1) at least some high-saturation IBPF present; (2) likely intermediate-saturation IBPF; (3) very slightly elevated resistivity and/or morphology that might indicate low-saturation IBPF; (4) equivocal interpretation and ice may or may not be present in pore space.

Oil and Gas Conservation Division, while the federal data and reports can be obtained from the Bureau of Safety and Environmental Enforcement (BSEE) in Anchorage, Alaska. The well coverage stretches from east of Barter Island to offshore Admiralty Bay (Figure 1), leaving the far western extent (near Barrow) and the far eastern extent (near the U.S.-Canada border) with few well constraints. Due to the logistical challenges of drilling in water-covered areas, many of the wells examined here were drilled on the extensive chains of barrier islands lying offshore the central U.S. Beaufort margin. Most of the wells were drilled to support petroleum exploration, meaning that their distribution is biased. Because many of the wells were planned by operators to penetrate 2000 m or more, the holes were often large (up to 67 cm) at the top, affecting the quality of some of the logs.

The borehole data set generally lacks well logs shallower than 30–50 m and is supplemented in the near surface by other geological and geophysical data sets. *Harding-Lawson Associates (HL)*, 1979] conducted a shallow (<35 m) geotechnical boring project that yielded some temperature logs and direct observations on recovered cores (Table 2). These observations are referred to here as "HL borings" with the corresponding identifier from Table 2. In addition, reports by *Horowitz* [2002] and *Northern Land Use Research (NLUR), Inc.* [2007] provide an overview of other unpublished information that constrains the presence of shallow permafrost in the vicinity of some OCS wells.

Considering both shallow geotechnical boring data [*HL*, 1979] and geophysical borehole logs means that different constraints on permafrost distribution are combined in this paper. *Collett and Bird* [1988] distinguish between permafrost (ground that has been held below the ice point for several years) and ice-bearing permafrost (IBPF), which refers to soil that contains ice that can be detected using geophysical

Table 2. Harding-Lawson Geotechnical Borings [*HL*, 1979] With Identification of Bonded (Cemented) Permafrost Zones and Descriptions of Temperature Measurements, Designated "T" in the Notes[a]

Borehole	Latitude (°N)	Longitude (°W)	Top Ice-Bonded Permafrost (m)	Base Ice-Bonded Permafrost (m)	Notes
HL1	70.41	−148.22			T increases then decreases to −1.4°C at ∼23.5 m
HL2	70.45	−148.45			T increases then decreases to −1.65°C at 23.3 m
HL3	70.53	−148.90			T increases then decreases to −1.9°C at ∼10 m
HL4	70.50	−148.38	12.2	12.3	T −1.5°C to −2°C measured to ∼20.4 m
HL5	70.51	−148.63			T <−1.5°C at top and ∼−2.7°C at ∼89 m
HL6	70.49	−148.13			T < −1.5°C at top and ∼−1.9°C at 31.5 m
HL7	70.45	−148.09			T increases to about −1.4°C at ∼6 m and then decreases to −1.7°C at 30.3 m
HL 8	70.50	−147.89	19.4	*30.5*	T remains between −1.5°C and −2°C to ∼29.5 m
HL9	70.38	−147.88	8.5	*39.6*	Complicated T structure...T increases to −1.5°C in much of section then ends −2°C at ∼38.6 m
HL10	70.45	−147.81	23.2	*32.9*	T increases to −1.5°C and remains stable to deepest measurement at ∼22.5 m
HL11	70.38	−147.68	24.1	*29.0*	T increases to −1.5°C and then decreases to −2°C at ∼28.7 m; "flammable gas"
HL12	70.44	−147.51	8.5	*91.7*	No ice bonding between 70 and 71 m; no T data
HL13	70.32	−147.65	9.5	*30.8*	No T data
HL14	70.28	−147.40			T increases to −1.4°C at ∼6.1 m and then decreases to −1.75°C at 29.6 m
HL15	70.22	−147.01	12.8	16.3	T first increases and then decreases steadily to −2.25°C at 89.5 m
HL16	70.27	−146.71	22.1	*33.5*	T first increases and then decreases steadily to −2.25°C at 32.6 m
HL17	70.27	−146.46	26.8	*31.5*	No T data
HL18	70.21	−146.04	12.5	*92.4*	T first increases then decreases steadily to −3.9 at 92 m
HL19	70.31	−146.97	23.8	*35.5*	No T data
HL20	70.37	−147.24	6.4	*34.6*	T first increases then decreases to −2°C at 30.8 m

[a]The borings are shown as triangles in Figures 3–6. An italicized base of ice-bonded permafrost indicates that the bottom of permafrost as reported corresponds to the deepest level attained in the boring. When no bonded sediments were recovered, top and base of ice-bonded permafrost are not reported.

methods [e.g., *Collett et al.*, 1988; *National Snow & Ice Data Center*, 2016]. The boring data provide both temperature logs and direct recovery of bonded (cemented) permafrost, according to the terminology of *HL* [1979], while the borehole logging data can only constrain IBPF. For many of the well logs examined here, the data can best be interpreted as indicating IBPF with low saturations of ice, but enough to still affect the geophysical signal. Particularly when discussing the implications of the observations, we do not hone strictly to the thermal definition of permafrost.

Owing to its focus on permafrost distribution, this analysis uses the uppermost 800 m of logging data from the boreholes. Since the thickest continuous IBPF-recorded onshore along the ANS is 670 m for the Prudhoe Bay area [*Collett et al.*, 1989], examination of the uppermost 800 m of the offshore records should yield accurate constraints on subsea permafrost. Data from more than 60 wells were examined, but fewer than 40 had a deep-formation resistivity log, which is considered the most diagnostic for IBPF, recorded shallower than ∼300 m. Some of the log files had been previously edited and published by P. Nelson and J. Kibler of the U.S. Geological Survey [e.g., *Nelson et al.*, 1999] for petroleum studies. However, the offshore wells have not been systematically analyzed for the constraints they place on the distribution of subsea permafrost beyond constraining the base of IBPF in pre-1990 wells [*Collett et al.*, 1989].

For this study, the primary indicator used to infer the presence of IBPF is elevated apparent resistivity as recorded by borehole electrical resistivity or induction logs. For the rest of the paper, we dispense with the term "apparent resistivity" and merely refer to "resistivity." Previous workers [*Collett et al.*, 1989] have adopted resistivity values (>1000 Ωm) to define zones characterized by IBPF, particularly for onshore ANS wells. This paper focuses on offshore wells, where permafrost is expected to be more degraded, very low resistivity seawater may sometimes act as one of the pore fluids, and saline waters may remain trapped in sediments in certain lithologies as a remnant of Pleistocene-era permafrost (and/or gas hydrate) formation (e.g., cryopeg). We therefore interpret offshore resistivity values of more than 100 Ωm as high-saturation IBPF, while also noting that several resistivity tools were used to acquire the logs and that values may not be directly comparable between wells. Resistivity log values between 10 and 100 Ωm yield an equivocal interpretation that could reflect the presence of limited ice in pore space, a freshwater lens, or a lithologic
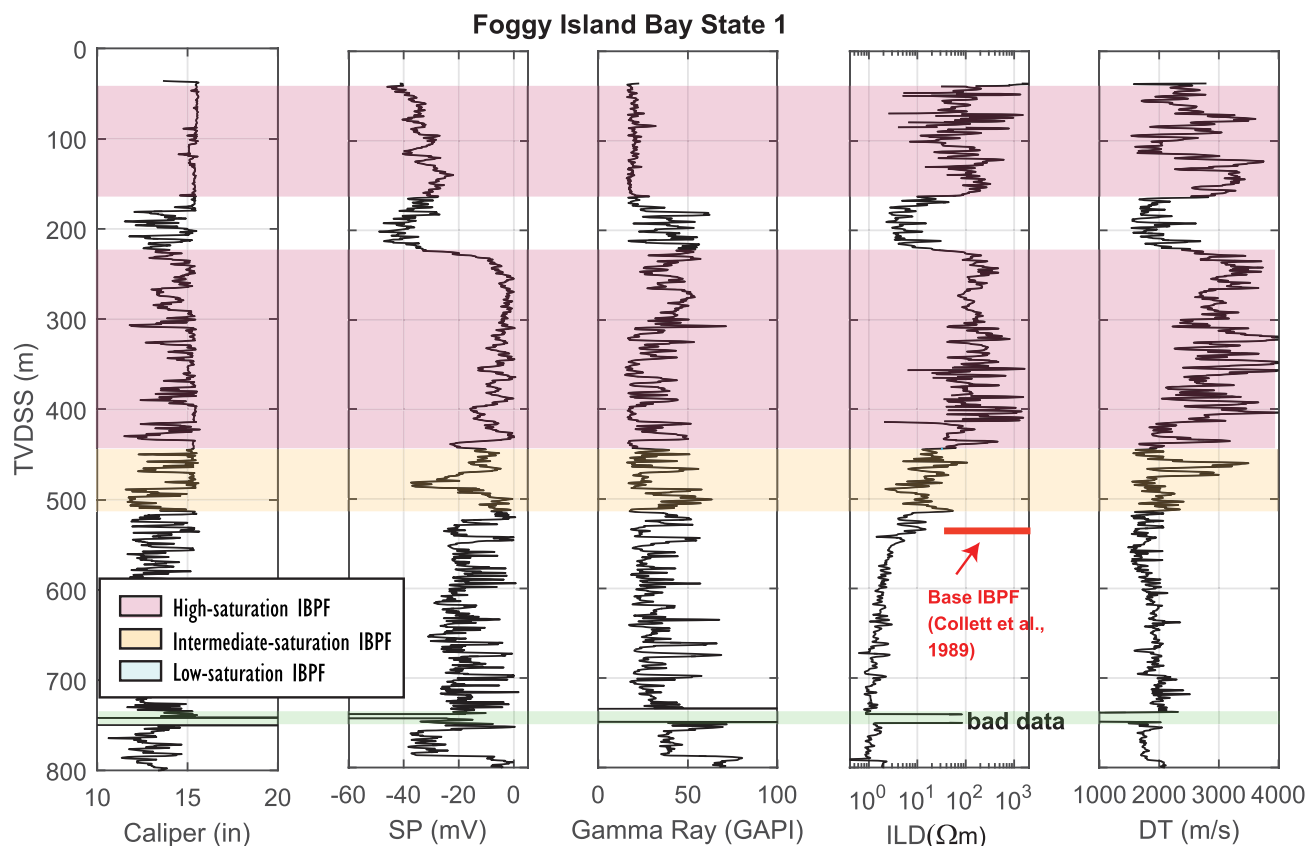
Figure 2. Borehole logging data from the Foggy Island Bay State 1 well, which is located onshore at Foggy Island Bay and which was previously interpreted by *Collett et al.* [1989] in their analysis of the base of IBPF (red line). The logs have been smoothed over 15 points (approximately 2.25 m) and are plotted against true vertical depth relative to sea level (TVDSS). The sonic log has been converted to seismic velocity from travel time as described in the text. Shading is indicated by the legend, and the resistivity values used to ascribe low-, intermediate-, and high-saturation IBPF are explained in the text.

change that causes resistivity to be locally elevated over background values. Here these are interpreted as intermediate-saturation IBPF. For a few wells in which the apparent resistivity is less than 10 Ωm, we infer the possibility of low ice content sediments (low-saturation IBPF) based on the qualitative morphology of the resistivity curve. Variability in shallow (<500 m) resistivities or increased resistivity values in this interval compared to the background values deeper in the hole are the subjective indicators used to tentatively infer that some IBPF may remain. We intuitively expect such morphologies for resistivity curves when there is thawing of pore-filling ice that may originally have existed at varying saturations as a function of depth in the shallow section.

The data set relies on deep resistivity/conductivity logs whose signals penetrate far enough into the formation away from the borehole that they should be unaffected by hole conditions or the presence of drilling mud. Most of the data set uses deep dual induction logs (ILD), an older type of electrical conductivity log. Some of the wells use phasor induction logs designated as IDP (deep phasor induction) or IDER (deep enhanced phasor induction). Induction data must be converted to resistivities and are unable to discriminate among very high resistivities (low conductivities). Other variations of deep resistivity/conductivity logs were reported in some cases, including modern deep-penetration laterologs (LLD), deep-penetration shielded electromagnetic wave resistivity (SEDP, EWDP), and induction resistivity (RILD). These logs all yield resistivities instead of conductivities. The labels in Figures 3–8 and Supporting Information retain the original designation of the logging tool.

After resistivity, the best indicator of the presence of IBPF is elevated seismic velocity. For spherical grains, acoustic velocity increases markedly when ice fills 40% of available pore space [e.g., *Zimmermann and King*, 1986; *Johansen et al.*, 2003]. At this saturation, water ice (or gas hydrate [*Yun et al.*, 2005]) binds the grains, enhancing the propagation of seismic energy through the sediments. Sonic logs (DT) recorded as travel time in μs ft^{-1} are converted to compressional wave velocities of m s^{-1} for the displays shown in Figure 2

and Supporting Information. Borehole logging sensors use ultrasonic frequencies, meaning that the absolute velocities they measure will not be directly comparable to field-scale velocities acquired using standard exploration seismic sources (i.e., 30–60 Hz). In this data set, high-saturation IBPF is associated with sonic logs close to 3000 m s^{-1}, slightly higher than the velocities of 2400–2800 m s^{-1} inferred for offshore IBPF at exploration seismic frequencies [e.g., *Brothers et al.*, 2016].

Collett et al. [1989] describe characteristic, but gradual, increases in spontaneous potential (SP; 20–30 mV) and gamma ray (GR; 5–10 API units) logs across the base of IBPF in their mostly onshore study. Since these indicators are more subtle than the changes in resistivity and seismic velocity, we do not rely on them as primary signs of remaining IBPF. Instead, these logs are invoked when they can be used to bolster the case for the presence of IBPF. When available, these logs are included in the individual well plots in Supporting Information.

Caliper logs provide information about the diameter of the borehole and therefore the expected degree of coupling between logging tools and the formation. For most of the wells examined here, caliper logs were not available or were incomplete in the shallow section. The paucity of such information hinders our ability to judge the quality of some of the borehole logs, particularly the sonic logs.

3. Results and Interpretations

To provide an example of a section containing known IBPF, we first present the borehole logs from a shoreline well interpreted by *Collett et al.* [1989]. Results for the remaining offshore wells are presented from east to west along the margin grouped by the geographic sectors shown in Figure 1.

3.1. Shoreline Example of IBPF

The Foggy Island Bay State 1 well is located onshore in the Sagavanirktok River Delta east of Prudhoe Bay and west of Foggy Island Bay. The well lies within 1 km distance of open water and is surrounded by inlets and small streams that comprise the delta. Because this well was previously analyzed by *Collett et al.* [1989], it provides calibration for the criteria used to delineate IBPF in this study. The base of IBPF was identified at 522 m by *Collett et al.* [1989], below a section with resistivity mostly in excess of 100 Ωm and seismic velocity greater than 2800 m s^{-1}. At the inferred base of IBPF, the SP log displays the subtle characteristic increase defined by *Collett et al.* [1989], although the gamma ray log does not. In our analysis, we interpret the thickest section of IBPF to be present between 230 and 440 m, with probable lower saturation IBPF present beneath this section and extending to ∼510 m (Figure 2). This lower ice content section may be attributable to freezing point depression due to salts, interaction with fine-grained sediments, or pore pressures [*Collett and Bird*, 1988] or to some thawing due to warming at the base of the permafrost.

As in most of the wells studied offshore on the Beaufort margin, IBPF is not continuous in the upper section of this well. For example, a sharp decrease in resistivity, seismic velocity, and SP and an increase in gamma ray signature between 170 and 230 m mark a cryopeg described by *Collett and Bird* [1993] and preclude IBPF with an ice content >40% [*Zimmermann and King*, 1986]; however, IBPF is clearly present at shallower depths. In this well, the top of the zone lacking IBPF may be traceable to a lithologic change at the base of the Pliocene section, but there is no clear lithologic explanation for the transition at ∼230 m. Correlations between ice content and lithologic changes are expected because fine-grained sediments often have low permeability and high capillary pressures that inhibit ice (and gas hydrate) formation [*Collett and Bird*, 1988; *Clennell et al.*, 1999]. Based on the information currently available, the lack of correlation between inferred IBPF signatures and known lithologic changes in this well is common across most of this data set.

3.2. Offshore Permafrost Assessment From Boreholes

The resistivity logs for wells that may contain an IBPF-related resistivity signal are presented in Figures 3–8 as a function of true vertical depth beneath the sea surface (TVDSS) when this value was provided (e.g., for nonvertical wells). Where TVDSS was not provided, it was calculated based on the well elevation, where available.

3.2.1. Eastern Sector

The eastern sector (Figure 3a) stretches from longitude 146.75°E through Camden Bay and eastward beyond Barter Island along a part of the margin that is distinguished by the relative absence of thermokarst lakes onshore and active compressional tectonism offshore [e.g., *Craig et al.*, 1985; *Grantz and May*, 1982]. On the western side of this sector, the back-barrier lagoon narrows from ∼5.4 km until the barrier islands
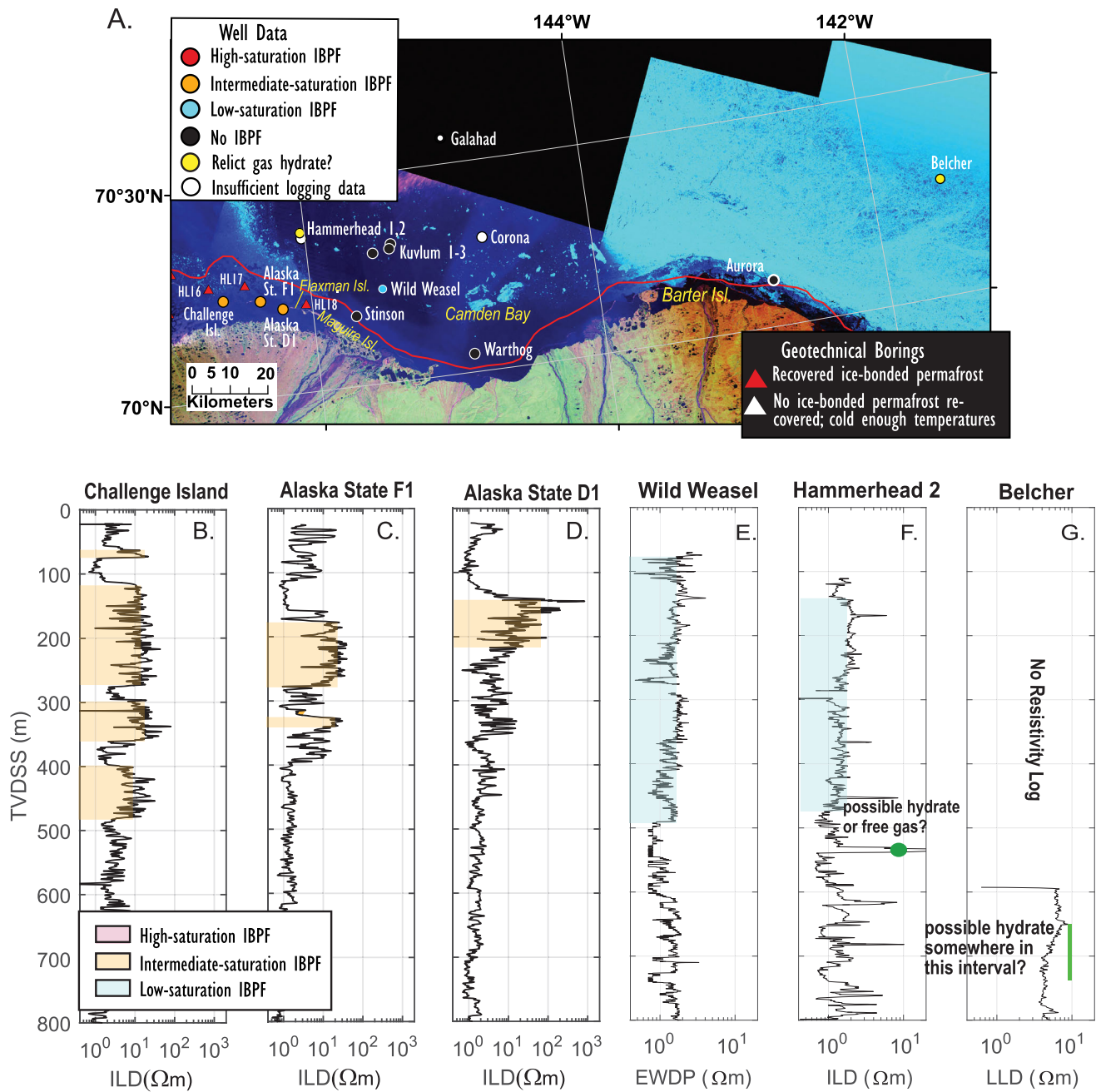
Figure 3. Interpreted resistivity logs for the area from Challenge Island to nearly the U.S.-Canada border. (a) Map showing compiled results. The red curve is the 2000 m s^{-1} velocity contour from the velocity analyses by *Brothers et al.* [2016]. Base map for this and other figures is from Landsat thematic mapper mosaics. (b–g) Resistivity logs for the wells in this area with IBPF zones marked. The resistivity values used to ascribe low-, intermediate-, and high-saturation IBPF are explained in the text. Note that logs in Figures 3e–3g are plotted at an expanded resistivity scale.

touch the mainland at the western end of Camden Bay. Where present within Camden Bay, the barrier islands lie mostly <2 km offshore. Passing eastward toward Barter Island, the barrier islands are close to or connected to the shore, implying that they have formed during sea level rise in the past few thousand years. The analyses of *Brothers et al.* [2012, 2016] indicate poorer IBPF preservation on this part of the margin than elsewhere, consistent with sustained exposure to the open ocean. Barrier island wells in this sector are confined to the westernmost and easternmost ends of the Maguire Islands (Challenge Island and Alaska State F1 on North Star Island, respectively) and to the western end of Flaxman Island (Alaska State D1). Open water OCS wells in this sector include Stinson, Wild Weasel, Warthog, Aurora, and some wells located farther offshore, including the multiple Hammerhead and Kuvlum wells and the outer shelf Galahad and Belcher wells.
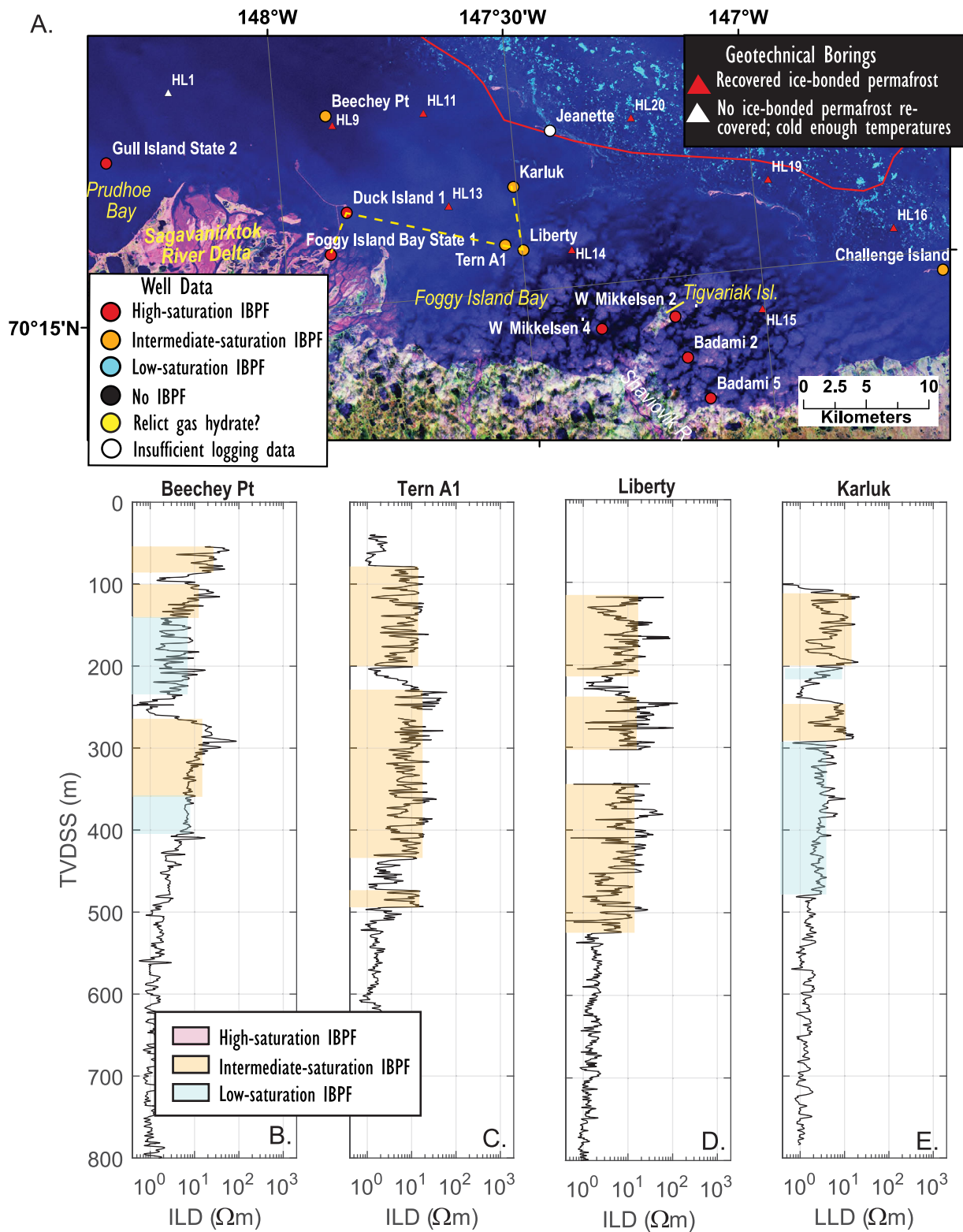
Figure 4. Interpreted resistivity logs from wells near Foggy Island Bay. (a) Map showing compiled results. The yellow dotted line shows the well transect used for the calculation of ice content in Figure 10a. The red curve is the 2000 m s^{-1} velocity contour from the velocity analyses by *Brothers et al.* [2016]. (b–e) Resistivity logs for some of the wells, with shading as given in the legend. The resistivity values used to ascribe low-, intermediate-, and high-saturation IBPF are explained in the text.
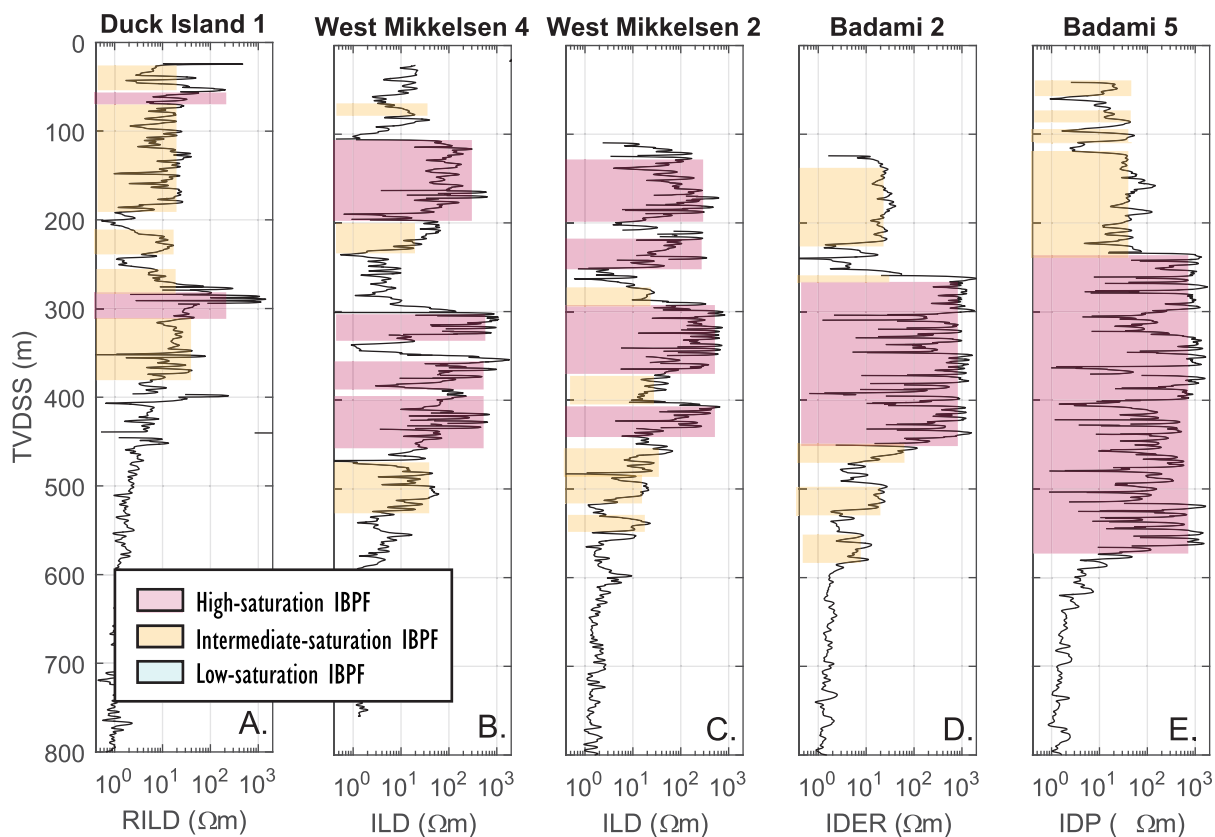
Figure 5. The remaining resistivity logs near Foggy Island Bay, with shading corresponding to IBPF saturations. The resistivity values used to ascribe low-, intermediate-, and high-saturation IBPF are explained in the text. The locations of these wells are shown in Figure 4a.

The Maguire Islands (Challenge and Alaska State F1 wells) have experienced a complex pattern of erosion and accretion that have resulted in a substantial net increase in their land area since the 1940s [*Gibbs and Richmond*, 2015]. Permafrost beneath the islands may therefore be relatively well-preserved since the ground surface is exposed to subzero temperatures for much of the year. The Challenge Island well (Figure 3b) has several zones of elevated resistivity, including a thin (10 m thick) interval at ∼70 m, a thick, intermediate interval (120–280 m), and two deeper, 60–80 m thick zones below ∼300 m and 400 m, respectively. The Alaska State F1 resistivity log (Figure 3c) shows an elevated signal that persists over most of the depth range between 180 and 340 m depth, except in a zone 40 m thick centered on 300 m. The sonic logs (Supporting Information) do not reveal corresponding seismic velocity increases, possibly due to the large diameter of the hole. Boring HL17 is located ∼6 km NNW and seaward of the Alaska State F1 well and contained only a ∼5 m thick layer of bonded permafrost in a zone at ∼31.6 m. No temperature log was available from HL17. Geotechnical boring HL16 is 5.4 km NW of the Challenge Island well and had 11 m of bonded permafrost starting at ∼22 m. The temperature near the bottom of this boring (∼32.5 m) was −2.25°C.

Flaxman Island, which hosts Alaska State Well D1, has near-surface features consistent with the presence of shallow permafrost (e.g., permafrost bluffs and thermokarst lakes) and a history of southward migration over the past six decades [*Gibbs and Richmond*, 2015]. The resistivity (Figure 3d) and sonic logs (Supporting Information) both increase between ∼140 and 215 m depth, indicating higher ice content than in the barrier island wells to the west. The SP and gamma ray logs show a decrease at the top of this zone, a signal consistent with an ice-free section over IBPF. Geotechnical boring HL18, located 6.25 km ENE of this well, recovered bonded permafrost from 12.5 to greater than 92 m and had temperatures of −3.9°C at 94 m depth.

The nearshore OCS wells on this part of the margin (Stinson, Warthog, and Aurora) lie less than 7 km offshore (Figure 3a), which is closer to the mainland than some barrier island wells that were drilled in the central sectors and that contain strong IBPF signatures (see below). Despite having well logs as shallow as
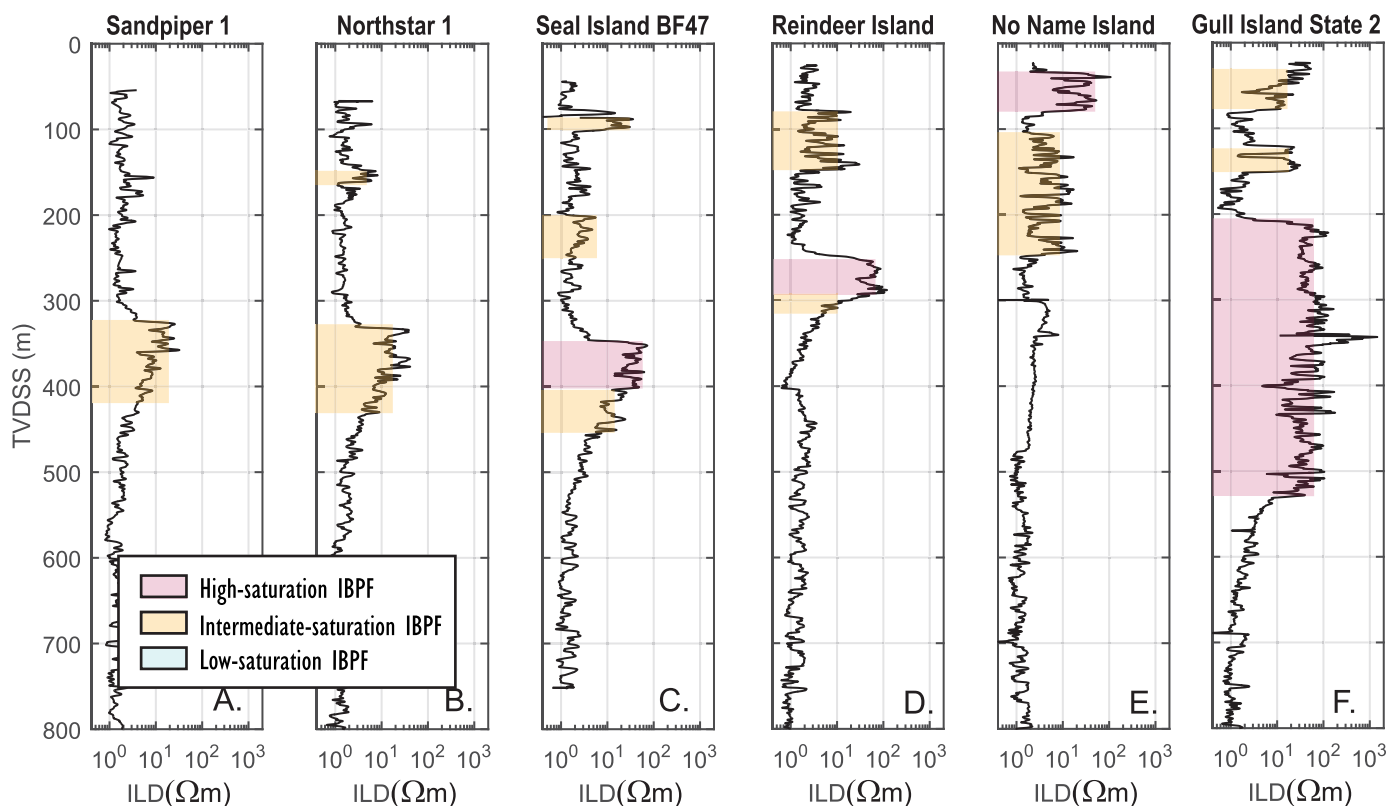
Figure 6. Interpreted resistivity logs from the Colville River Delta to Prudhoe Bay. (a) Map showing compiled results. The red curve is the 2000 m s^{-1} velocity contour from the velocity analyses by *Brothers et al.* [2016]. (b–f) Resistivity logs for the nearshore wells, with shading corresponding to the interpreted IBPF intervals. The resistivity values used to ascribe low-, intermediate-, and high-saturation IBPF are explained in the text.

Figure 7. The remaining wells in the Colville River Delta to Prudhoe Bay area, with an emphasis on the wells that are farther offshore (except for Gull Island State 2). The resistivity values used to ascribe low-, intermediate-, and high-saturation IBPF are explained in the text. The locations of these wells are shown in Figure 6a.

250–300 m, none of the nearshore OCS wells in this sector reveals evidence for IBPF. The open ocean location of these wells, as well as the relatively deep (∼20 m) water depth for the Aurora well, may have exposed the seafloor in these areas to a longer history of inundation and possible seawater infiltration, leading to substantial permafrost degradation. This is at odds with the inference of shallow subseafloor permafrost near the Warthog [*NLUR*, 2007] and Aurora [*Horowitz*, 2002] wells. No HL geotechnical borings were completed this far to the east.

Farther offshore in this sector are OCS wells (Table S1) Wild Weasel (26.5 m water depth), Kuvlum 1-3 (30.8–33.5 m water depth), Hammerhead 1 and 2 (average 32.6 m water depth), and Corona (35.4 m water depth). Corona and Hammerhead 1 lack logs shallower than ∼800 m. The Kuvlum wells were logged deeper than ∼300 m, but the resistivity data at the top of this zone reveal no indication of IBPF. The Wild Weasel well has resistivity less than 5 Ωm in the upper part of the section, but the morphology of the curve between 80 and 210 m could tentatively suggest minor amounts of low-saturation IBPF (Figure 3e).

The Hammerhead 2 well is a special case. The resistivity curve (Figure 3f) in the shallow section has morphology similar to that in the Wild Weasel well and thus provides the same equivocal interpretation for low-saturation IBPF. The most notable feature in this well is anomalously high resistivity at 533 m. This feature was interpreted by *Collett et al.* [2011] as possible methane hydrate or associated free gas that is stratigraphically correlative with an onshore gas hydrate occurrence. Gas hydrate could only have formed at this location if it had originally been within or beneath permafrost.

Another special case in this sector is the Belcher well (Figure 3g), which lies in ∼50 m water on the outer shelf east of the Aurora well. Gas hydrate was recovered on the rig floor when this well had been drilled to ∼754 m depth, and the hydrate-bearing siltstone described in the well report could have originated at this depth or shallower in the well. The well report also speculates that the gas hydrate may have been capped by permafrost, which could explain some of the gas flow observations during drilling. Taken together, the Hammerhead and Belcher results imply that permafrost may once have persisted more than 50 km from the present-day shoreline across the Beaufort shelf in the eastern sector.
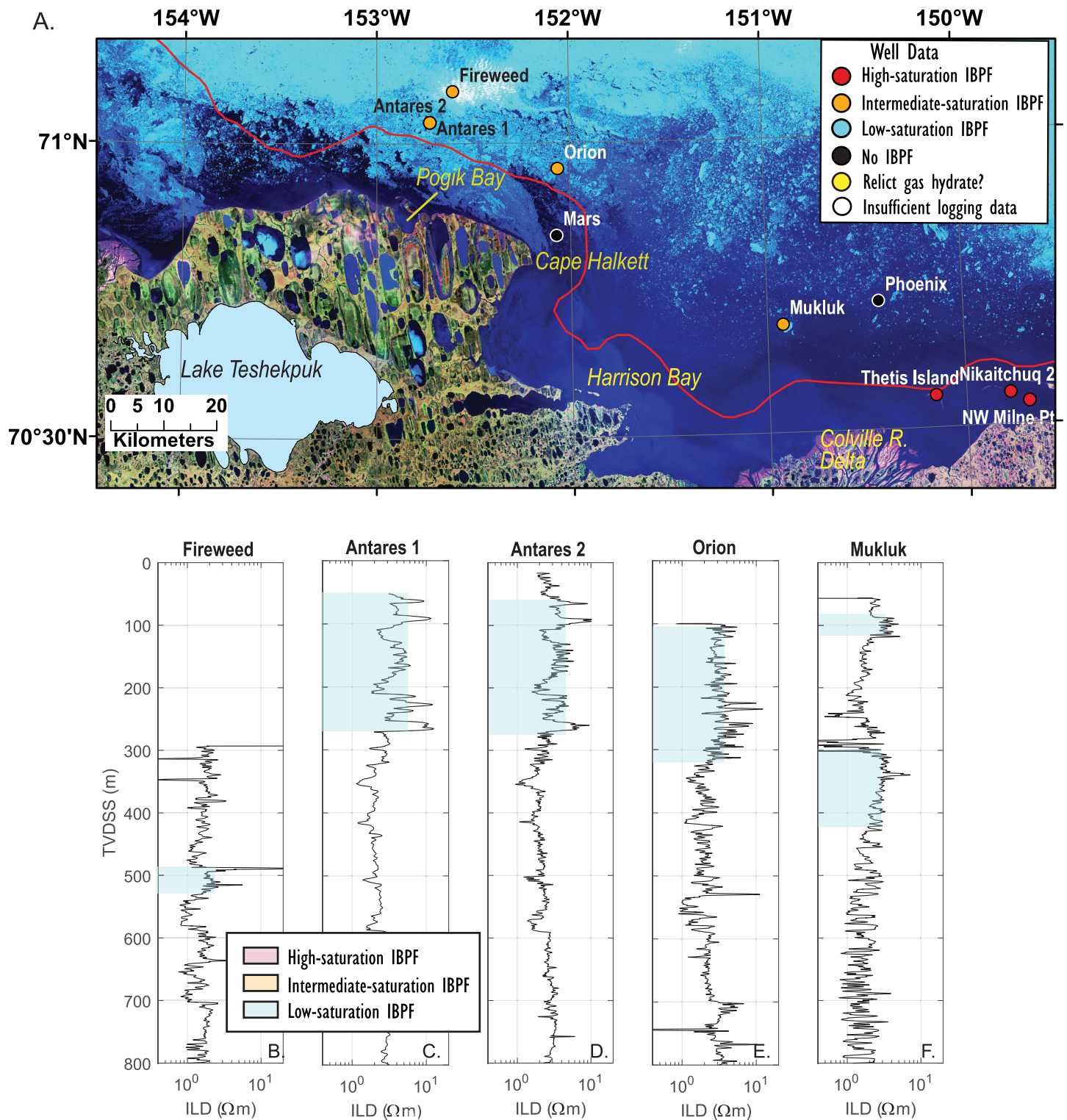
Figure 8. (a) Compiled results for the analysis of IBPF signatures in OCS wells in the Pogik Bay to Colville River Delta sector. The red curve is the 2000 m s^{-1} velocity contour from the velocity analyses by *Brothers et al.* [2016]. (b–f) Interpreted borehole resistivity logs. The resistivity values used to ascribe low-, intermediate-, and high-saturation IBPF are explained in the text. Note that these logs are plotted at an expanded resistivity scale relative to other figures in the paper.

3.2.2. Foggy Island Bay Sector

This sector stretches from the Sagavanirktok River Delta on the west to longitude 146.75°E and is the site of 10 wells (Figure 4a), nearly all of which show indications of IBPF present in the shallow sedimentary section. The main barrier islands on this part of the margin lie more than 10 km offshore, but the wells are concentrated on nearshore islands and in the lagoon between the shoreline and the main barrier islands.

The Tern A1, Liberty, and Karluk OCS wells were drilled in the middle of Foggy Island Bay, with the Karluk well located ∼4.8 km seaward of Tern A1, which is in turn only ∼2 km WNW of the Liberty well. At a comparable position to Karluk relative to the barrier islands, but closer to shore and due north of the Sagavanirktok River, is the Beechey Point OCS well. Among these wells, evidence for IBPF is weakest in the Karluk well, which is the farthest offshore. The Karluk resistivity log (Figure 4e) reveals slightly elevated values between the top of the log and ∼480 m although the sonic log shows no corresponding increase. The resistivity and sonic log signals, coupled with the position of this well, may indicate low-saturation IBPF and possibly saline intrusion through some parts of the sedimentary section. The Tern A1 logs show elevated, near-constant resistivity (Figure 4c) in zones between 80 and 200 m, 240 and 440 m, and 470 and 495 m, again without an associated seismic velocity increase. In the Liberty well (Figure 4d), the zone of elevated resistivity is more continuous and is correlated with increases in seismic velocities that cannot be connected to known lithologic changes. The Beechey Point well (Figure 4b) shows two zones of elevated resistivity, the first starting at ∼50 m depth and a stronger signal starting at 260 m, where the increased resistivity correlates with higher seismic velocities. The pattern of elevated (>10 Ωm) resistivities in the Liberty, Tern, and Beechey Point #1 well are consistent with the presence of intermediate- to high-saturation IBPF, some of which remains intact enough (>40% ice saturation) to also increase seismic velocities. Geotechnical boring HL13, which lies 5.5 km ENE of the Tern well, encountered bonded permafrost between 9.5 and 30.8 m. HL14, located 3.8 km east of the Liberty well, recovered no bonded permafrost, but a temperature of −1.75°C was measured at 29.6 m. The Beechey Point well is within 1 km of HL9, where permafrost was present from 8.5 to the base of the hole (39.6 m) and temperatures near the bottom of the boring were −2°C.

Closer to shore or on islands located close to the shoreline in this sector are the Duck Island, West Mikkelsen State Unit 2 and 4, and the Badami 2 and 5 wells (Figure 5), all of which have strongly elevated resistivity logs (and usually correlative increases in seismic velocity) indicative of intermediate to high-saturation IBPF in the shallow sedimentary section. Of these wells, Duck Island (Figure 5a), located on a strip barrier offshore Foggy Island State 1 borehole (Figure 2), has the most difficult signal to interpret in terms of IBPF, possibly due to its proximity to the Sagavanirktok River outfall [e.g., *Hopkins and Hartz*, 1978]. The rest of the nearshore wells were drilled on (West Mikkelsen 2) or offshore (West Mikkelsen 4) Tigvariak Island, a low-elevation remnant tundra island that is close to the shoreline in the Shaviovik River delta [*Gibbs and Richmond*, 2015]. Despite their similar geographic position relative to the coastline, the zones of elevated resistivity in the West Mikkelsen 2 well (Figure 5c) are more continuous and have higher values than those in the Duck Island strip barrier island well, likely reflecting differences in lithology, the geology of the islands, and/or possibly the inundation history for these two wells. The West Mikkelsen 4 well log (Figure 5b) is most similar to that of West Mikkelsen 2 and also has IBPF through much of the section from 100 to 450 m and sections of inferred lower saturation IBPF deeper than 450 m. Boring HL15 is 6.9 km to the east of the West Mikkelsen 2 well and approximately the same distance from the shoreline as that well. Permafrost was encountered in the first 20 m of that boring, and the temperature at ∼90 m depth was −2.25°C, low enough to sustain permafrost if sufficient water and coarse lithologies were present. Taken together, the observations provide strong evidence for lateral continuity of permafrost-bearing sediments in shallow offshore waters in this sector.

The Badami 2 well, which lies ∼3 km offshore the mainland, and the Badami 5 well, which was drilled right at the shoreline, are east of Tigvariak Island. Both wells have thick, continuous sections of IBPF deeper than 260 and 230 m, respectively, with possible lower saturation IBPF through much of the section shallower than 200 m (Figures 5d and 5e). The contour map of *Collett et al.* [1989] indicates that the base of IBPF in this area should be greater than 425 m, which is consistent with the resistivity data in all of the wells in this sector except the nearshore Badami 5, where the IBPF extends even deeper (575 m).

3.2.3. Colville River to Sagavanirktok River

This sector stretches from the Colville River Delta on the west and then across Prudhoe Bay, ending at the Sagavanirktok River on the east (Figure 6a). Eleven boreholes (Figures 6 and 7) had sufficient logging data to evaluate the presence of IBPF.

On the western side of the sector, the wells on Thetis Island, the Spy Islands (Nikaitchuq wells), and the Jones Islands (Jones Island well on former Bodfish Island and the Long Island well) sample barrier islands from the Colville Delta to nearly the Kuparuk River. All of these islands have experienced rapid change in their sedimentary regimes over the past seven decades, meaning that the borehole logs represent a snapshot in their histories. For example, Thetis Island has migrated 800 m west and 730 m south [*Gibbs and Richmond*, 2015] since 1947. The Jones Islands, classified as a tundra remnant with significant topography, have merged to form a single strip barrier, while the Spy Islands split into two, migrated south, and experienced net accretion during that period [*Gibbs and Richmond*, 2015].

The resistivity logs for the four barrier island wells (Figures 6b, 6c, 6e, and 6f) indicate increased preservation of IBPF from west to east, with the IBPF section reaching at least 200 m thick in the Jones and Long Island wells (Figures 6e and 6f). The sections both above and below the high-saturation IBPF ($\sim$370–460 m) in the Thetis Island well likely contain lower saturation IBPF, although no sonic log is available as verification. Permafrost beneath Thetis Island may be affected both by the relative warmth of the Colville River discharge and potential downcutting that exposes the subsurface to saline intrusion [*Hopkins and Hartz*, 1978]. The Nikaitchuq well has multiple intervals of IBPF, particularly deeper than $\sim$440 m, but the noisy nature of this log renders further interpretation difficult.

The Northwest Milne Point well (Figure 6d) was drilled in the lagoon between Milne Point (mainland) and the Spy Islands. The resistivity log implies that IBPF (475–505 m) or lower saturation IBPF (150–170 m; 360–410 m, and 520–570 m) may be present through most of the section. The sonic log (Supporting Information) is elevated only in the inferred high saturation IBPF interval. The measured resistivity in the section immediately overlying the deepest IBPF interval is the lowest in the entire data set, possibly indicating a cryopeg.

The outer barrier islands in this sector lie seaward of the Jones Islands and Long Island and, from west to east, are the locations of the Sandpiper (Loon Shoal), Northstar 1, Seal Island BF-47, Reindeer Island, and No Name Island wells (Figure 7). Seal Island BF-47, which is not the same as the OCS wells of this name, and the Northstar 1 well, which is not associated with the North Star Island in the Maguire chain (site of Alaska State Well F1; Figure 3c), may lie on the western continuation of the line of islands that include Cross, Reindeer, and Argo. These older barrier islands are 11–19 km offshore, of different morphology, and of different orientation than the nearshore barriers and are undergoing rapid change. For example, between 1947 and 2006, the mid-twentieth century Reindeer Island disappeared, but the island's total landmass grew by more than 100% while experiencing up to 500 m of migration to the southwest, extension to the west by up to 1 km, and a split into two masses [*Gibbs and Richmond*, 2015]. This pattern of rapid change underscores that the well, which was abandoned in 1979, captures conditions at a discrete time and place in the history of the shallow sedimentary section beneath the island. Similarly, the No Name Island well is located on the former Bartlett Island, which was located off the southwest tip of Cross Island before the islands merged during the last six decades [*Gibbs and Richmond*, 2015]. The Beaufort Sea Block 54-1 well was drilled at the northern end of Cross Island, but not logged shallower than $\sim$1000 m and does not appear Table 1.

The primary IBPF signature in the Sandpiper, Northstar 1, and Seal Island wells (Figure 7a–7c) is relatively deep in the section ($>$320 m) and up to 100 m thick, with the top of IBPF deepening from west to east. In the Seal Island well, this zone corresponds to a decrease in seismic velocity (Supporting Information), although the lack of a caliper log in this large-diameter part of the hole makes the seismic signal difficult to interpret. In both the Northstar 1 and Seal Island wells, 20–50 m thick zones with elevated resistivity shallower than 100 and 250 m, respectively, might also represent IBPF. In the Reindeer Island well (no sonic log; Figure 7d), the IBPF zone is shallower than 295 m, and resistivity is elevated in a 70 m thick section starting at $\sim$70 m depth, where we infer intermediate ice saturation. Focusing on the better-quality part of the No Name Island resistivity log (shallower than 300 m), IBPF appears to be present within 100 m of the surface, and IBPF with lower ice content may occupy an 150 m thick zone below that (Figure 7e). Of these outer barrier island wells, No Name Island has IBPF through the thickest section, perhaps reflecting the long-term stability of this site close to Cross Island.

The final well in this sector is Gull Island State 2 (Figure 7f), located on a small island just outside the mouth of Prudhoe Bay. The resistivity log shows a strong IBPF signal between $\sim$210 m and 520 m and a corresponding decrease in the SP log at the base of the zone. The contour map published by *Collett et al.* [1989] also places the base of IBPF at $\sim$520 m at this location. This well has one of the best sections of vertically

continuous IBPF of any drilled offshore on the U.S. Beaufort margin. The closest HL boring is 7.5 km seaward and had temperatures that could sustain permafrost, although no samples were recovered.

Geotechnical boring HL3 was taken 1.6 km to the east of Northstar 1. Bonded permafrost was not recovered from this short borehole, but the temperature is $-1.9°C$ at $\sim$10 m depth. Technical boring HL5 is $\sim$3 km seaward of the Seal Island well, and no permafrost was recovered from the boring, which was one of the deepest completed. However, the temperature at $\sim$89 m depth was $-2.7°C$, which would be consistent with permafrost conditions if lithology, saturation conditions, and pore water salinities permitted. Shallow permafrost and a temperature of $-2°C$ at $\sim$20 m were encountered in HL4, located less than 3 km away from Reindeer Island.

3.2.4. Pogik Bay to the Colville River

No barrier islands shield the coast in this sector, and the only wells available to constrain subsea permafrost are OCS wells located more than 15 km offshore in open water (Figure 8a). These wells include Antares 1 and 2, $\sim$17 km offshore Pogik Point, and Fireweed, $\sim$5.5 km farther offshore; the Orion well offshore Cape Halkett; and the Mukluk well located more than 20 km offshore the Colville River Delta. The Antares wells are examples for which the evidence for low-saturation IBPF is based not only on the resistivity values (almost uniformly less than 10 Ωm), but rather also on the morphology of the curves. In the Antares 1 well (Figure 8c), mildly elevated resistivity is observed from 120 to 270 m. The Antares 2 well (Figure 8d) has elevated resistivity from 60 to 325 m, with corresponding increases in seismic velocity only in the interval of 65–100 m. The signal in the Fireweed well (Figure 8b) is even more subtle, with barely elevated resistivity and sonic velocities in a zone from 470 to 510 m. In the Orion well (Figure 8e), a subtle increase in resistivity over background levels is observed shallower than 320 m (log starts at $\sim$100 m) and may also represent low-saturation IBPF. The sonic velocities (Supporting Information) in this interval are barely elevated over background values, also implying that the ice content is relatively low in the section. The weakest evidence for IBPF is from the Mukluk well (Figure 8f), which has an interval of slightly elevated resistivity values from 90 to 120 m and overall decreasing resistivity with depth between 300 and 420 m. There are no corroborating seismic data for this part of the Mukluk well, and the interpretation remains speculative. The *NLUR* [2007] report refers to the shallow (near-seafloor) permafrost in the vicinity of the Fireweed well. *Horowitz* [2002] describes bonded permafrost in two shallow boreholes close to the Orion well and shallow permafrost in the vicinity of the nearby Mars OCS well, where no borehole logs are available for the upper 450 m.

3.2.5. Boreholes Lacking Data or a IBPF Signatures

The OCS wells that lack suitable logging data or have no IBPF signatures are detailed in Supporting Information Table S1. Some of the wells in which we identify no IBPF signal based on resistivity logs may in fact intersect very low saturation IBPF that has dramatically degraded from its original state due to warming or saline intrusion. Figure S15 plots available logs for the Galahad (outer shelf) and Aurora (midshelf) wells, whose locations are shown in Figure 3a. Both wells have low-resistivity values throughout and certainly lack IBPF now. The Galahad resistivity log has a very slightly elevated signature in the shallow section, and the morphology is consistent with other logs in which we have inferred remaining IBPF at a saturation too low ($<$40%) to have a marked impact on bulk resistivity values. However, the interpretation of low-saturation IBPF for the Galahad well would be far more speculative than for wells nearer the shore, and we lack nearby borings or other geophysical data that could be used as a secondary indicator of IBPF. To provide confidence in the interpretation, methods other than borehole logging would be required to detect remaining ice at very low saturations in sedimentary sections inundated relatively early in the post-LGM inundation episode.

4. Discussion

The data compiled here provide the first comprehensive overview of direct borehole constraints on the occurrence of subsea permafrost along a $\sim$500 km long part of the U.S. Beaufort Sea margin stretching from Pogik Bay to nearly the U.S.-Canada border. The results also yield insights into along-margin and shore-perpendicular variations in the current state of subsea permafrost and can be compared with subsea permafrost distributions inferred from regional-scale seismic analyses [*Brothers et al.*, 2012, 2016]. The analysis also has implications for permafrost distribution beneath the present-day continental shelf at the end of the Last Glacial Maximum, which in turn may provide hints about the fate of subsea permafrost under a regime of continued future global warming.

4.1. Patterns of Contemporary Subsea Permafrost Distribution

A few generalizations emerge from the borehole data analysis, which is summarized in Figure 9. The locations closer to the present-day shoreline or on tundra islands in the nearshore have the best preserved permafrost, as expected for inundation proceeding from the outer to inner shelf since ∼15 ka. IBPF degrades seaward within ∼15 km and is mostly retained in layers less than 100 m thick at depths greater than 200–300 m. While widespread well control is lacking seaward of the barrier islands, the available logs show that IBPF signatures are rarely present seaward of the main barrier islands, and then mostly at sites like Reindeer Island, which were drilled on an older, outlying island chain. Despite their proximity to the shoreline, lagoonal wells offshore Milne Point and in Foggy Island Bay generally have thinner IBPF sections and inferred lower ice saturations than barrier islands that lie seaward of them, possibly attesting to the vulnerability of permafrost to thawing and seawater intrusion once it has been inundated, even by shallow waters. Gull Island in Prudhoe Bay and Badami 5 east of Tigvariak Island are exceptions, but they also lie in the nearshore in areas known to have the thickest onshore IBPF on the ANS [*Collett et al.*, 1989] and where inundation has likely occurred only since a few thousand years ago [e.g., *Lachenbruch et al.*, 1982].

While the offshore borehole data presented here are skewed towards barrier islands, these islands also play a critical role in subsea permafrost dynamics along much of this margin. Tundra remnant islands often have shallow permafrost, including near-surface ice-bonded sediments, that make them more resistant to erosion and that insulate and protect underlying shallow permafrost. Low-lying clastic barrier islands that migrate up to a few meters a year can also temporarily insulate and preserve a core of underlying permafrost.

The absence of IBPF signatures in most wells seaward of the barrier islands and on parts of the coastline unprotected by barrier islands (e.g., west of Harrison Bay) could alternately indicate a lithologic change to finer-grained material that excluded the formation of IBPF in the first place [e.g., *Collett and Bird*, 1988]. This is the same possibility raised by *Brothers et al.* [2012] in analyzing refraction results that indicated a limited offshore extent for IBPF. A simpler explanation is that the lack of IBPF-related log signals in the open ocean settings may reflect the effects of inner shelf inundation over 12–15 ka [*Hill et al.*, 1985]. Flooding of the inner shelf by ocean waters may have provided enough warming to thaw the sedimentary section at the open ocean sites so that not even signals associated with low-saturation IBPF remain.
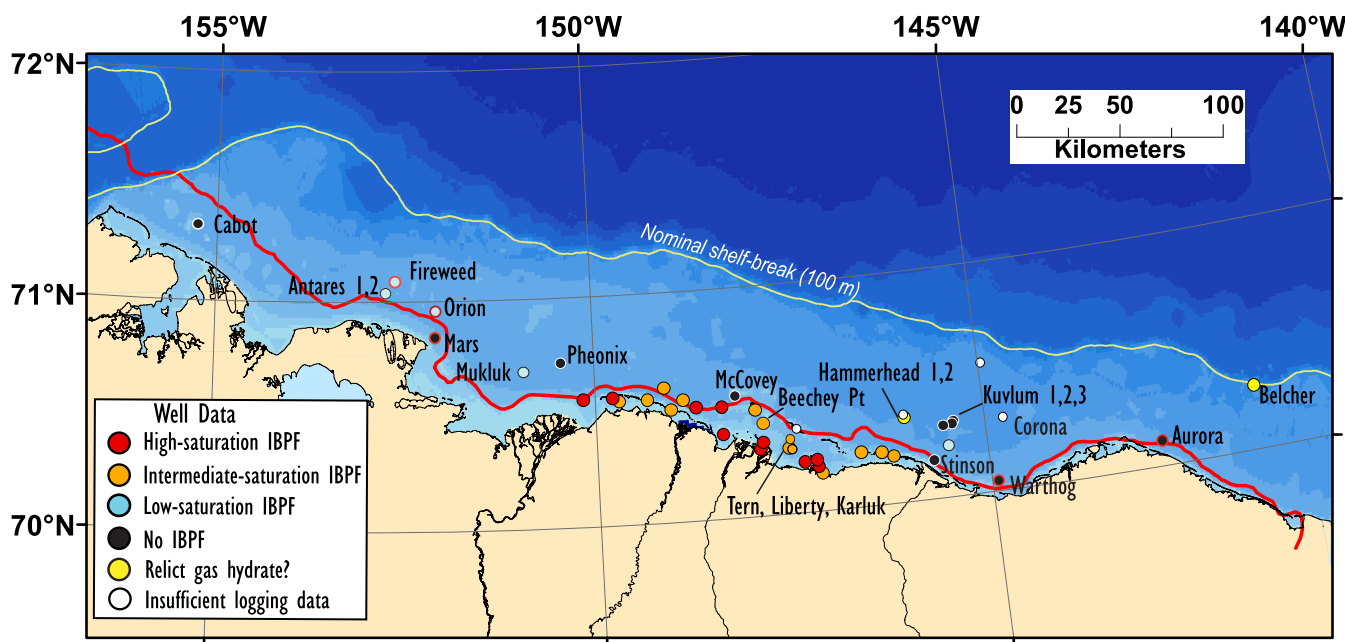

Figure 9. Compilation of all resistivity log interpretations on the U.S. Beaufort margin relative to the 2000 m s^{-1} velocity contour that is inferred to mark the seaward extent of IBPF from the analyses by *Brothers et al.* [2016]. Red rims on circles indicate that near-seafloor permafrost was described at these locations by *Horowitz* [2002] or *NLUR* [2007].

4.2. Comparison With Seismic Results

The spatial pattern inferred for IBPF distribution based on the compiled borehole logs (Figure 9) correlates well with the results from velocity analyses of 100,000 km of industry exploration seismic reflection data on the U.S. Beaufort shelf [*Brothers et al.*, 2016]. The 2000 m s^{-1} bulk velocity contour (red curve in Figures 1, 3a, 4a, 6a, and 8a) was calculated by *Brothers et al.* [2016] using the entire section within 750 ms two-way travel time (TWTT). They interpreted this contour as a proxy for the seaward termination of continuous IBPF based on the abrupt change in velocity structure seaward of that contour. A bulk velocity of 2000 m s^{-1} would correspond to ∼684 m depth below the seafloor for a nominal water depth of 15 m and assumed background sediment velocity of 1875 m s^{-1}, meaning that the full depth range over which onshore permafrost exists [*Collett et al.*, 1989] is captured. Using an arithmetic mixing relationship of the form adopted by *Brothers et al.* [2016]:

$$2000 \; m/s = x \cdot v_{IBPF} + [1-x] \cdot 1875 \; m/s, \tag{1}$$

where *x* is the fraction of the section that has IBPF seismic velocity of v_{IBPF} and 2000 and 1875 m s^{-1} correspond to the velocity at the assumed seaward extent of IBPF and the velocity of background sediments, respectively, it is possible to calculate the proportion of IBPF in the sedimentary section within the 750 ms TWTT interval. Note that (1) is independent of the thickness of the section sampled by a 750 ms TWTT. For the 2000 m s^{-1} contour to represent the 40% ice saturation threshold [*Zimmermann and King*, 1986], the velocity ascribed to sections with low-saturation IBPF only needs to be ∼2185 m s^{-1}, which is a plausible in light of the velocities inferred by *Brothers et al.* [2016]. Based on resistivity logs, some boreholes well within the 2000 m s^{-1} contour, such as those in inner Foggy Island Bay (Figure 5), on some barrier islands (Figures 6e and 6f), and the Gull Island State well (Figure 7f), clearly meet the criterion and possess the required percentage of IBPF in the sedimentary section above 700 m. Wells farther offshore in Foggy Island Bay (Figures 4b–4e), just east of the Colville River Delta (Figures 6b and 6d), and Challenge Island (Figure 3b) also have sufficient IBPF in this depth interval to produce seismic velocities in excess of 2000 m s^{-1}. Seaward of the 2000 m s^{-1} contour, none of the wells has resistivity signatures that would indicate the presence of enough IBPF to produce elevated seismic velocities. Overall, the borehole data confirm that the 2000 m s^{-1} contour from *Brothers et al.* [2016] represents a reliable indicator of the offshore persistence of significant thicknesses of IBPF.

Another approach for interpreting the borehole logs is to calculate the saturation (occupied percentage of pore space) of ice in each well based on the inferred porosity and the deep resistivity logs. The first step in determining ice saturation is typically calculation of porosity from density logs, which we lack. The shallow section is usually drilled with large diameter holes that are then washed out to create an even larger borehole, and density logging tools do not provide reliable data under such conditions (T. Collett, personal communication). Instead, we use an empirical porosity (φ) versus depth (*z*) function derived for wells with IBPF onshore in the Prudhoe Bay area by *Lee* [2005]: $\phi = 0.532 e^{-z/1963}$, where *z* is in meters. The saturation *S* of ice and/or gas hydrate in pore space can then be determined from the assumed porosity function and the measured borehole apparent resistivity (R_0) using

$$S = 1 - \left(\frac{aR_w}{\phi^k R_0} \right)^{1/n}. \tag{2}$$

In (2), *k* is the cementation factor, here taken as 2, and aR_w, which denotes a constant multiplied by the apparent resistivity of water-saturated sediments, is assigned a value of 1 Ωm, as in *Lee* [2005]. These parameters lie within the bounds provided from an analysis of near-seafloor sediments from the Bering Strait [*Boyce*, 1968]. In (2), *n* is taken as 1.9386 after *Pearson et al.* [1983] and in accordance with approach of *Lee* [2005].

Along a transect through four wells from the onshore Foggy Island Bay State well to the Karluk well (Figure 4a), the total thickness of the section with high ice content decreases dramatically, as does the average ice content for each well (Figure 10a). The 40% ice saturation line shown on the plots in Figure 10a corresponds to the threshold beneath which seismic velocity is not expected to be affected by the presence of ice in pore space [*Zimmermann and King*, 1986]. Notably, the Liberty well, in which less than half the section has inferred ice content greater than 40%, has elevated seismic velocity logs (Supporting Information). The Karluk well logs show no seismic velocity increases, consistent with the inferred ice content generally being
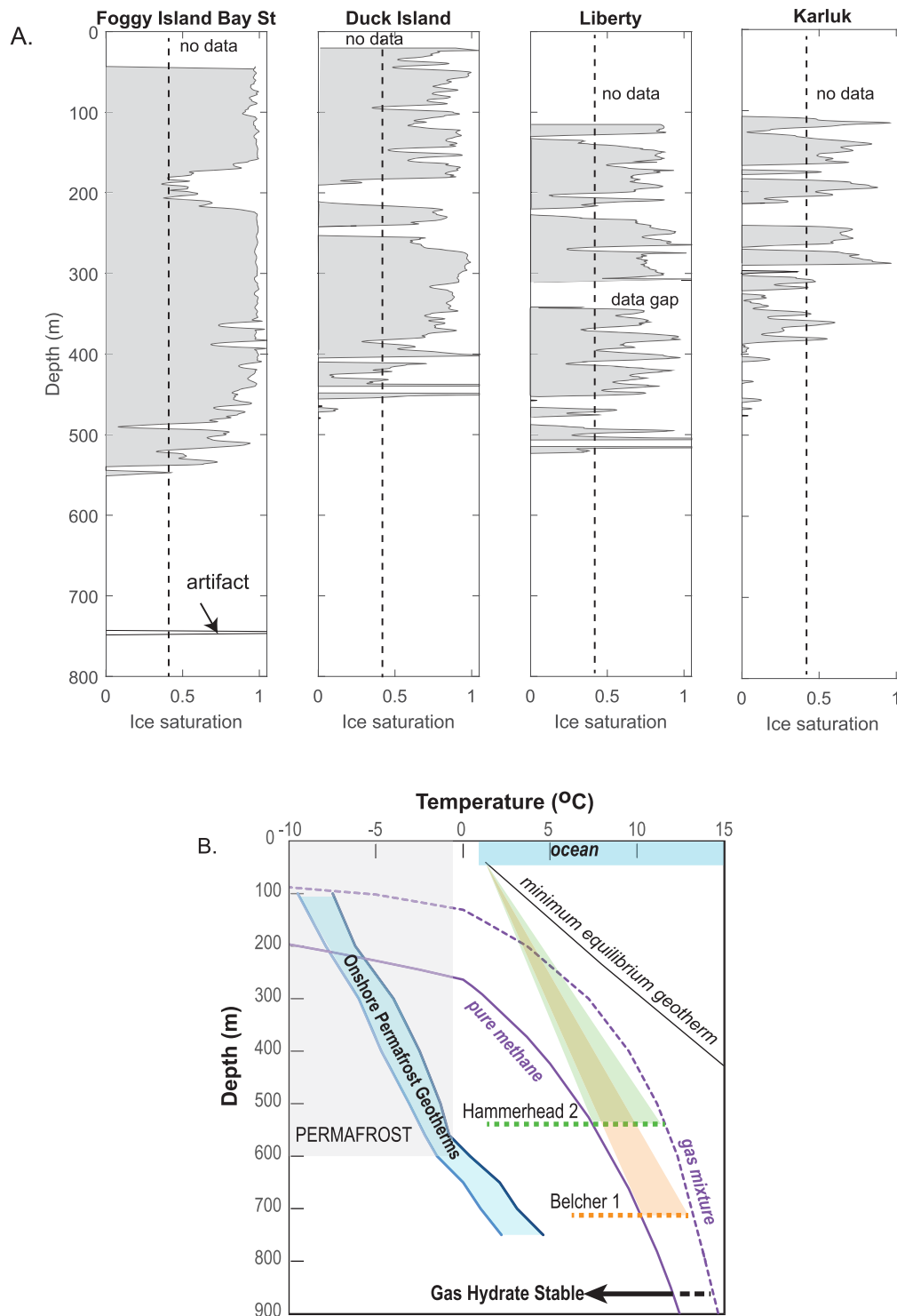
Figure 10. (a) Ice saturation calculated as a fraction of pore space in four wells along the transect shown by the dotted yellow line in Figure 4a. The dashed line corresponds to 40% saturation of ice in pore space. (b) Gas hydrate may be present in the Hammerhead 1 well [*Collett et al.*, 2011] at 533 m depth (green dashed line) and was recovered in the Belcher 1 well at 754 m depth (orange dashed line). These gas hydrate occurrences are shown relative to the gas hydrate stability boundaries for pure methane hydrate (solid purple line) and a mixture of methane, CO_2, and higher hydrocarbon gases (dashed purple line) found at a well on the shores of Harrison Bay [*Lorenson and Collett*, 2011]. The shaded green area shows the maximum average linear geotherms possible for gas hydrate to remain stable at the Hammerhead well, and the shaded orange area shows the same for the Belcher well. For reference, a nominal minimum equilibrium geotherm of 35 mK/m (without permafrost) is shown as the dashed black line. The ocean geotherms assume seafloor temperature of 1.5°C. For comparison, the blue shaded area on the left side of the diagram shows Prudhoe Bay onshore permafrost geotherms from *Lachenbruch et al.* [1982].

lower than 40%. For this study, we do not independently convert seismic velocities to inferred ice saturations owing to the relatively poor quality of some of the velocity logs in the shallow section where hole diameters are generally large.

We also calculated S using a simpler relationship that has been used in some gas hydrate studies and that is not explicitly dependent on assumed porosity [*Collett and Ladd*, 2000]: $S = 1 - (R_w/R_0)^{1/n}$. For this expression, R_w was chosen by averaging log values in an 100–150 m interval deeper than 750 m, yielding values between 0.997 and 1.226 Ωm for the four wells plotted in Figure 10a. Using this relationship yields significantly higher ice saturations than (2) and predictions of ice beneath the base of IBPF. We conclude that the approach outlined in (2) is better for this first attempt at calculating ice saturations from legacy borehole logging data.

4.3. Constraints on Paleodistribution of Subsea Permafrost

The preservation of subsea permafrost in the contemporary record depends on how much was present at the onset of inundation, as well as the timing of inundation. Without direct analysis of grain deformation and sediment texture, determining the a priori thickness of offshore permafrost is not possible. The signal associated with IBPF in the wells whose logs are shown in Figures 3–8 never continues deeper than 450–570 m, whereas the base of onshore permafrost is as deep as 670 m depth [*Collett et al.*, 1989] along the onshore area where many of the wells are concentrated. In the limit, IBPF that currently persists offshore could have been as thick as that onshore at the LGM. In this case, the observations made in this paper may be consistent with both top-down and bottom-up thawing, features often noted in numerical models [e.g., *Pokrovsky*, 2003; *Taylor et al.*, 2013]. If the now-subsea permafrost were never as thick as the onshore permafrost, then the argument for bottom-up thawing becomes more equivocal.

Since the Prudhoe Bay subsea permafrost study of *Lachenbruch et al.* [1982], researchers have surmised that differential inundation has been critical in permafrost preservation offshore the central U.S. Beaufort shelf. The pattern of preservation that we infer here is consistent with most of the mid- and outer shelf having been inundated earlier [e.g., *Hill et al.*, 1985] and having undergone more permafrost degradation than the innermost shelf, where inundation may date from only a few thousand years ago [*Lachenbruch et al.*, 1982]. Permafrost also appears to be more degraded on the eastern side of the margin than in the central section, possibly because the eastern wells are more exposed to the open ocean than the wells in the Prudhoe and Foggy Island Bay area. Comparable conclusions are harder to infer west of the Colville River because no suitable wells are available closer to shore.

Equivocal gas hydrate indicators in the Hammerhead 1 [*Collett et al.*, 2011] and Belcher 1 wells might imply that permafrost was once widespread beneath the present-day shelf on the eastern side of the study area. As shown in Figure 10b, for gas hydrate to currently be preserved in an equilibrium state at 533 m depth at Hammerhead 1 requires a maximum average thermal gradient of 11–21 mK m^{-1} for end-member gas hydrate compositions (methane only and one that includes thermogenic gases [*Lorenson and Collett*, 2011], respectively). The maximum thermal gradients consistent with the Belcher 1 discovery of gas hydrate at 754 m maximum depth are 11 to 15 mK m^{-1} for the same gas mixtures. The heat flow reported by *Lachenbruch et al.* [1982] for the Prudhoe Bay area and the map generated by *Phrampus et al.* [2014] across the Beaufort shelf yield estimated shelf thermal gradients of 35–55 mK m^{-1}, depending on the thermal conductivity adopted. Clearly, the thermal gradients required for the preservation of gas hydrate at the Belcher 1 and Hammerhead 1 wells are far lower than the inferred regional values and not much different from gradients observed onshore in Prudhoe Bay wells characterized by thick permafrost [*Lachenbruch et al.*, 1982]. If gas hydrate were present at Hammerhead 1 and Belcher 1, it probably formed within and beneath permafrost, respectively. Although any relict gas hydrate deposit is likely not in an equilibrium thermal state, the possibility that gas hydrate might be preserved in the contemporary record still requires such low thermal gradients that a regime of continuing thermal equilibration of shelf sediments following subsea permafrost thaw is the most plausible explanation for the existence of gas hydrate.

5. Conclusions

The borehole data examined here confirm with direct measurements the inferences made about the lateral distribution of subsea IBPF on the U.S. Beaufort margin based on regional seismic studies [*Brothers et al.*,

2012, 2016]. Namely, subsea permafrost is confined within a few tens of kilometers of the present-day shoreline and at water depths less than a few tens of meters. Intact, thick sections of subsea IBPF are present only in wells drilled close to the present-day shoreline. The strip barrier islands between Camden Bay and the Colville River mostly lie above sedimentary sections that contain IBPF that is confined to zones several hundred meters deep and rarely more than 200 m thick, consistent with substantial top-down thawing since the onset of inundation. Lagoonal areas behind the barrier islands tend to have more degraded IBPF than the islands, while IBPF indicators are lacking seaward of the strip barrier islands except just west of Prudhoe Bay. The best preserved IBPF is in wells in Prudhoe Bay and east of the Sagavanirktok River.

When coupled with the borehole and seismic reflection and refraction analyses conducted on the adjacent Canadian Beaufort margin [e.g., *Hunter and Hobson*, 1974; *Hu et al.*, 2013], this and the other recent U.S. Beaufort margin regional-scale studies [*Brothers et al.*, 2012, 2016] represent the final steps in using existing, publicly available data to describe the contemporary state of subsea permafrost in the Western Arctic Ocean. Further efforts to describe the subtleties of lateral and vertical variations in subsea permafrost on this margin will require new drilling or seismic data acquisition or an analysis of privately held seismic data sets. Such research should not only cover a larger regional extent than has been possible so far, but also compare newly acquired information to the baseline interpretations from legacy borehole (this paper) and seismic [*Brothers et al.*, 2016] data in an effort to constrain subsea permafrost loss over the past few decades.

References

Bekryaev, R. V., I. V. Polyakov, and V. A. Alexeev (2010), Role of polar amplification in long-term surface air temperature variations and modern arctic warming, *J. Clim.*, *23*, 3888–3906.

Boyce, R. E. (1968), Electrical resistivity of modern marine sediments from the Bering Sea, *J. Geophys. Res.*, *73*(14), 4759–4766, doi:10.1029/JB073i014p04759.

Brothers, L. L., P. E. Hart, and C. D. Ruppel (2012), Minimum distribution of subsea ice-bearing permafrost on the U.S. Beaufort Sea continental shelf, *Geophys. Res. Lett.*, *39*, L15501, doi:10.1029/2012GL052222.

Brothers, L. L., B. M. Herman, P. E. Hart, and C. D. Ruppel (2016), Subsea ice-bearing permafrost on the U.S. Beaufort Margin: 1. Minimum seaward extent defined from multichannel seismic reflection data, *Geochem. Geophys. Geosyst.*, *17*, doi:10.1002/2016GC006584, in press.

Brown, J., O. J. Ferrians Jr., J. A. Heginbottom, and E. S. Melnikov (Eds.) (1997), Circum-Arctic map of permafrost and ground-ice conditions, *Circum-Pac. Map Ser. CP-45*, 1 sheet, scale 1:10,000,000, U.S. Geol. Surv. in Coop. with the Circum-Pac. Counc. for Energy and Miner. Resour., Washington, D. C.

Clennell, M. B., M. Hovland, J. S. Booth, P. Henry, and W. J. Winters (1999), Formation of natural gas hydrates in marine sediments: 1. Conceptual model of gas hydrate growth conditioned by host sediment properties, *J. Geophys. Res.*, *104*(B10), 22,985–23,003, doi:10.1029/1999JB900175.

Collett, T. S., and K. J. Bird (1988), Freezing-point depression at the base of ice-bearing permafrost of the North Slope of Alaska, in *5th International Conference on Permafrost*, pp. 50–57, Tapir Publ., Tronheim, Norway.

Collett, T. S., and K. J. Bird (1993), Unfrozen, high-salinity intervals within ice-bearing permafrost, North Slope of Alaska, in *6th International Conference on Permafrost*, pp. 1-7, South China Univ. of Technol. Press, Beijing.

Collett, T. S., and J. W. Ladd (2000), Detection of gas hydrate with downhole logs and assessment of gas hydrate concentrations (saturations) and gas volumes on the Blake Ridge with electrical resistivity log data, in *Proceedings of the Ocean Drilling Program, Scientific Results*, edited by C. K. Paull et al., vol. 164, pp. 1–13, Ocean Drill. Program, College Station, Tex.

Collett, T. S., K. J. Bird, K. A. Kvenvolden, and L. B. Magoon (1988), Geologic interrelations relative to gas hydrates within the North Slope of Alaska, *U.S. Geol. Surv. Open File Rep.*, *88-389*, 150 pp.

Collett, T. S., K. J. Bird, K. A. Kvenvolden, and L. B. Magoon (1989), Map showing the depth to the base o fthe deepest ice-bearing permafrost as determined from well logs, North Slope, Alaska, *U.S. Geol. Surv. Oil Gas Invest. Map, 222*, 1 sheet, scale 1:10,000,000, U. S. Geol. Surv., North Slope, Alaska.

Collett, T. S., M. W. Lee, W. F. Agena, J. J. Miller, K. A. Lewis, M. V. Zyrianova, R. Boswell, T. L. Inks (2011), Permafrost associated natural gas hydrate occurrences on the Alaskan North Slope, *Mar. Pet. Geol.*, *28*, 279–294.

Craig, J. D., K. W. Sherwood, and P. P. Johnson (1985), Geologic report for the Beaufort Sea planning area, Alaska: Regional geology, petroleum geology, environmental geology, *OCS Rep. MMS, 85-0111*, 192 pp.

Fairbanks, R. G. (1989), A 17,000-year glacio-eustatic sea level record; influence of glacial melting rates on the Younger Dryas event and deep-ocean circulation, *Nature*, *342*(6250), 637–642.

Gibbs, A. E., and B. M. Richmond (2015), National assessment of shoreline change—Historical shoreline change along the north coast of Alaska, U.S.–Canadian border to Icy Cape, *U.S. Geol. Surv. Open File Rep.*, *2015–1048*, 96 pp.

Grantz, A., and S. D. May (1982), Rifting history and structural development of the continental margin north of Alaska, in *Studies of Continental Margin Geology*, edited by J. S. Watkins and C. L. Drake, *AAPG Mem.*, *34*, 77–102.

Harding-Lawson Associates (HL) (1979), *USGS Technical Investigation Beaufort Sea-1979*, 2 vols., 452 pp.

Hill, P. R., P. J. Mudie, K. Moran, and S. M. Blasco (1985), A sea-level curve for the Canadian Beaufort Shelf, *Can. J. Earth Sci.*, *22*, 1383–1393.

Hopkins, D. M., and R. W. Hartz (1978), Coastal morphology, coastal erosion, and barrier islands of the Beaufort Sea Alaska, *U.S. Geol. Surv. Open File Rep.*, *78-1063*, 58 pp.

Horowitz, W. L. (2002), Evaluation of sub-sea physical environmental data for the Beaufort Sea OCS and incorporation into a Geographic Information System (GIS) database, *OCS Study MMS 2002-017*, 76 pp.

Hu, K., Z. Issler, Z. Chen, and T. A. Brent (2013), Permafrost investigation by well logs, and seismic velocity and repeated shallow temperature surveys, Beaufort-Mackenzie Basin, *Geol. Surv. Can. Open File Rep.*, *6956*, 228 pp.

Hunter, J. A., and G. D. Hobson (1974), Seismic refraction method of detecting sub-seabottom permafrost, in *The Coast and Shelf of the Beaufort Sea*, edited by J. C. Reed and J. E. Sater, pp. 401–415, Arctic Inst. of North Am., San Francisco, Calif.

Hunter, J. A., K. G. Neave, H. A. MacAulay, and G. D. Hobson (1978), Interpretation of sub-seabottom permafrost in the Beaufort Sea, in *Third International Conference on Permafrost* edited by C. B. Crawford, pp. 514–520, Natl. Res. Counc. of Can., Edmonton, Canada.

Johansen, T. A., P. Digranes, M. van Schaack, and I. Lonne (2003), Seismic mapping and modeling of near-surface sediments in polar areas, *Geophysics*, 68, 566–573.

Kang, S.-G., J. K. Hong, Y. K. Jin, S. Kim, Y.-G. Kim, M. Riedel, S. Dallimore, and C. Shin (2015), P-wave velocity models using full waveform inversion for the permafrost in the Canadian shelf of the Beaufort Sea, Arctic, Abstract B31D-0588 presented at 2015 AGU Fall Meeting, San Francisco, Calif., 14–18 Dec.

Lachenbruch, A., J. H. Sass, B. V. Marshall, and T. H. Moses Jr. (1982), Permafrost, heat flow, and the geothermal Regime at Prudhoe Bay, Alaska, *J. Geophys. Res.*, 87(B11), 9301–9316, doi:10.1029/JB087iB11p09301.

Lee, M. W. (2005), Well log analysis to assist the interpretation of 3-D seismic data at the Milne Point, North Slope of Alaska, *U.S. Geol. Surv. Sci. Invest. Rep.*, 2005–5048, 18 pp.

Lorenson, T. D., and T. S. Collett (2011), Gas hydrate prospecting using well cuttings and mud-gas geochemistry from 35 wells, North Slope, Alaska, *U.S. Geol. Surv. Sci. Invest. Rep.*, 2011-5195, 27 pp.

National Research Council (NRC), Marine Board (1983), Understanding the Arctic sea floor for engineering purposes, *Spec. Rep., 83-25*, 153 pp.

National Snow & Ice Data Center (2016), Cryosphere Glossary. [Available at https://nsidc.org/cryosphere/glossary/, last accessed 28 Sept 2016.]

Neave, K. G., and P. V. Sellman (1984), Determining distribution patterns of ice-bonded permafrost in the U.S. Beaufort sea from seismic data, in *The Alaskan Beaufort Sea: Ecosystems and Environments*, edited by P. W. Barnes, D. M. Schell, and E. Reimnitz, pp. 237–258, Academic, Orlando, Fla.

Nelson, P. H., J. E. Kibler, and C. P. Giberson (1999), Well data and well plots, *U.S. Geol. Surv. Open File Rep.*, 98-34, 84 pp.

Northern Land Use Research (NLUR), Inc. (2007), Final report: Review of geological/geophysical data and core analysis to determine archaeological potential of buried landforms, Beaufort Sea Shelf, Alaska, *OCS Study MMS, 2007-004*, 74 pp.

Paull, C. K., W. Ussler III, S. R. Dallimore, S. M. Blasco, T. D. Lorenson, H. Melling, B. E. Medioli, F. M. Nixon, and F. A. McLaughlin (2007), Origin of pingo-like features on the Beaufort Sea shelf and their possible relationship to decomposing methane gas hydrates, *Geophys. Res. Lett.*, 34, L01603, doi:10.1029/2006GL027977.

Paull, C. K., et al. (2015), Active mud volcanoes on the continental slope of the Canadian Beaufort Sea, *Geochem. Geophys. Geosyst.*, 16, 3160–3181, doi:10.1002/2015GC005928.

Pearson, C. F., P. M. Halleck, P. L. McGuire, R. Hermes, and M. Mathews (1983), Natural gas hydrate deposits: A review of in-situ properties, *J. Phys. Chem.*, 87, 4180–4185.

Phrampus, B. J., M. J. Hornbach, C. D. Ruppel, and P. E. Hart (2014), Widespread gas hydrate instability on the upper U.S. Beaufort margin, *J. Geophys. Res. Solid Earth*, 119, 8594–8609, doi:10.1002/2014JB011290.

Pithan, F., and T. Mauritsen (2014), Arctic amplification dominated by temperature feedbacks in contemporary climate models, *Nat. Geosci.*, 7, 181–184, doi:10.1038/ngeo2071.

Pokrovsky, S. I. (2003), Modeling permafrost and gas hydrate stability zones within Alaskan Arctic shelves and continental margins, MS thesis, 136 pp., Geophys. Inst., Univ. of Alaska Fairbanks, Fairbanks.

Portnov, A., A. J. Smith, J. Mienert, G. Cherkashov, P. Rekant, P. Semenov, P. Serov, and B. Vanshtein (2013), Offshore permafrost decay and massive seabed methane escape in water depths >20 m at the South Kara Sea shelf, *Geophys. Res. Lett.*, 40, 3962–3967, doi:10.1002/grl.50735.

Portnov, A., J. Mienert, and P. Serov (2014), Modeling the evolution of climate-sensitive Arctic subsea permafrost in regions of extensive gas expulsion at the West Yamal shelf, *J. Geophys. Res. Biogeosci.*, 119, 2082–2094, doi:10.1002/2014JG002685.

Portnov, A., S. Vadakkepuliyambatta, J. Mienert, and A. Hubbard (2016), Ice-sheet-driven methane storage and release in the Arctic, *Nat. Commun.*, 7, Article 10314, doi:10.1038/ncomms10314.

Rachold, V., D. Y. Bolshiyanov, H.-W. Hubberton, R. Junker, V. V. Kunitsky, F. Merker, P. P. Overduin, and W. Schneider (2007), Near-shore Arctic subsea permafrost in transition, *Eos Trans. AGU*, 88(13), 149–156.

Rekant, P., G. Cherkashev, B. Vanstein, and P. Krinitsky (2005), Submarine permafrost in the nearshore zone of the southwestern Kara Sea, *Geo Mar. Lett.*, 25(2–3), 183–189.

Romanovskii, N. N., A. V. Gavrilov, V. E. Tumskoy, A. L. Kholodov, C. Siegert, H.-W. Hubberten, and A. V. Sher (1998), Environmental evolution in the Laptev Sea region during Late Pleistocene and Holocene, *Polarforschung*, 68, 237–245.

Ruppel, C. (2011), Methane hydrates and contemporary climate change, *Nat. Educ. Knowledge*, 2(12), 12. [Available at http://www.nature.com/scitable/knowledge/library/methane-hydrates-and-contemporary-climate-change-24314790]

Shakhova, N., I. Semiletov, I. Leifer, A. Salyuk, P. Rekant, and D. Kosmach (2010), Geochemical and geophysical evidence of methane release over the East Siberian Arctic Shelf, *J. Geophys. Res.*, 115, C08007, doi:10.1029/2009JC005602.

Taylor, A. E., S. R. Dallimore, P. R. Hill, D. R. Issler, S. Blasco, and F. Wright (2013), Numerical model of the geothermal regime on the Beaufort Shelf, arctic Canada since the Last Interglacial, *J. Geophys. Res. Earth Surf.*, 118, 2365–2379, doi:10.1002/2013JF002859.

Yun, T. S., F. Francisca, J. C. Santamarina, and C. Ruppel (2005), Compressional and shear wave velocities of uncemented sediment containing gas hydrate, *Geophys. Res. Lett.*, 32, L10609, doi:10.1029/2005GL022607.

Zimmermann, R. W., and M. King (1986), The effect of the extent of freezing on seismic velocities in unconsolidated permafrost, *Geophysics*, 51, 1285–1290.